Environmental Science & Technology

Article

Cite This: Environ. Sci. Technol. 2018, 52, 7775−7784

pubs.acs.org/est

Geostatistical Prediction of Microbial Water Quality Throughout a Stream Network Using Meteorology, Land Cover, and Spatiotemporal Autocorrelation

David A. Holcomb,[†] Kyle P. Messier,[‡] Marc L. Serre,[†] Jakob G. Rowny,[†] and Jill R. Stewart*[,†]

[†]Department of Environmental Sciences and Engineering, Gillings School of Global Public Health, University of North Carolina, Chapel Hill, North Carolina 27599-7431, United States

[‡]Department of Civil, Architectural, and Environmental Engineering, University of Texas, Austin, Texas 78712, United States

Supporting Information

ABSTRACT: Predictive modeling is promising as an inexpensive tool to assess water quality. We developed geostatistical predictive models of microbial water quality that empirically modeled spatiotemporal autocorrelation in measured fecal coliform (FC) bacteria concentrations to improve prediction. We compared five geostatistical models featuring different autocorrelation structures, fit to 676 observations from 19 locations in North Carolina's Jordan Lake watershed using meteorological and land cover predictor variables. Though stream distance metrics (with and without flow-weighting) failed to improve prediction over the Euclidean distance metric, incorporating temporal autocorrelation substantially improved prediction over the space-only models. We predicted FC throughout the stream network daily for one year, designating locations "impaired", "unimpaired", or "unassessed" if the probability of exceeding the state standard was ≥90%, ≤10%, or >10% but <90%, respectively. We could assign impairment status to more of the stream network on days any FC were measured, suggesting frequent sample-based monitoring remains necessary, though implementing spatiotemporal predictive models may reduce the number of concurrent sampling locations required to adequately assess water quality. Together, these results suggest that prioritizing sampling at different times and conditions using geographically sparse monitoring networks is adequate to build robust and informative geostatistical models of water quality impairment.

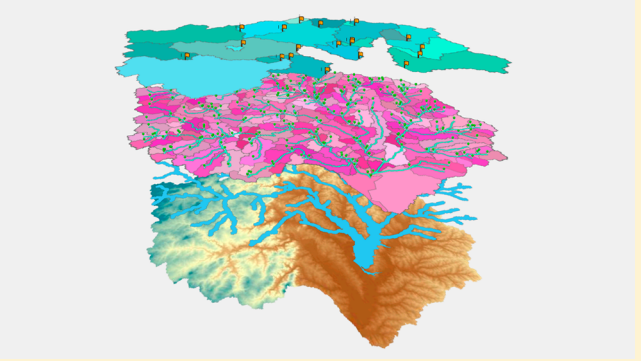

INTRODUCTION

Fecal contamination introduces pathogens to water bodies that can impact human health upon contact or ingestion, with outcomes including gastrointestinal, skin, and respiratory illness.[1,2] Even limited contact with impacted water bodies has been associated with adverse health outcomes.[3] It is not feasible to directly measure the numerous fecal-source pathogens that may be present in aquatic environments, so traditional water quality monitoring relies on the enumeration of fecal indicator bacteria (FIB) such as fecal coliform (FC) bacteria, *Escherichia coli*, or *Enterococcus* spp. Health risks associated with contacting waters impacted by fecal pollution, as indicated by the presence of FIB, are well documented but may vary with the source of fecal pollution.[4−8]

Despite efforts to mitigate fecal pollution from point sources, pathogen contamination as measured by FIB remains the leading cause of impairment for United States water bodies reported under Section 303 (d) of the Clean Water Act.[9,10] The dramatic increase in FIB concentration routinely observed during and after storm events, as well as associations with land use patterns and geology, suggests that nonpoint source (NPS) fecal pollution is a major contributor to microbial water quality impairment.[11−16] Traditional monitoring strategies, which rely on infrequent grab sampling, cannot capture the rapid changes in water quality that arise under systems dominated by NPS pollution.[16−19] Responding to these limitations, predictive statistical modeling has been suggested as an inexpensive tool to supplement sample-based monitoring.[20−22]

By characterizing the relationships between FIB and other environmental factors, predictive models can be used to estimate FIB concentrations at unmonitored locations and times. Applications of predictive modeling include forecasting, nowcasting, expanding the coverage of routine monitoring, and investigating the patterns and determinants of contamination to inform management efforts.[21,23−25] A common approach is simple empirical modeling, in which the association between FIB and a set of comeasured predictors is estimated. These

Received: March 2, 2018
Revised: June 9, 2018
Accepted: June 10, 2018
Published: June 11, 2018

DOI: 10.1021/acs.est.8b01178
Environ. Sci. Technol. 2018, 52, 7775−7784

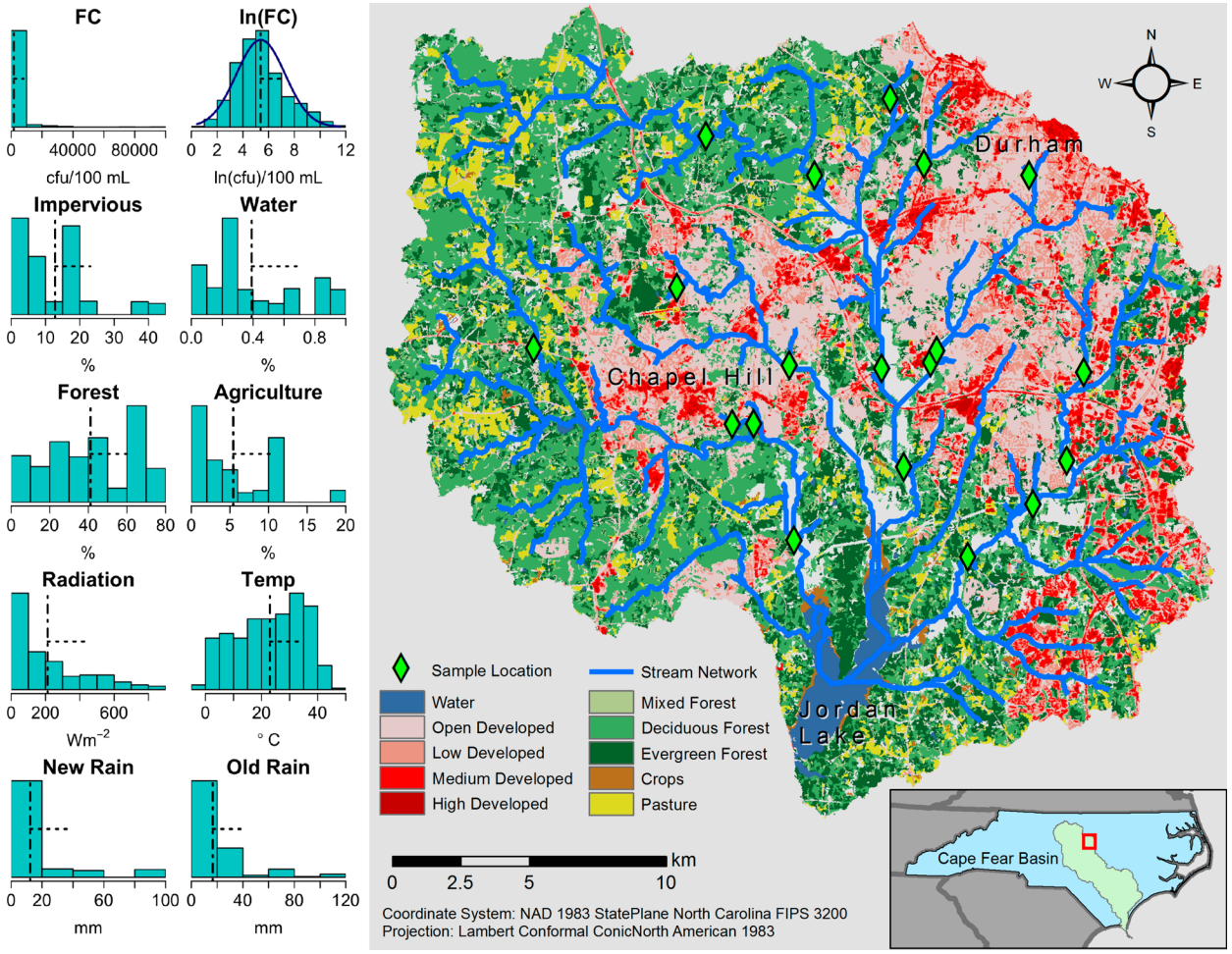

Figure 1. Input variable distributions (frequency histograms), sampling locations (diamonds), stream network (blue polyline), and land cover classification (colored raster cells) in the Jordan Lake near-upstream watershed in central North Carolina. Sample means (vertical dot-dashed lines) and standard deviations (horizontal dotted lines) are indicated for each input variable, calculated from 676 observations; note the approximate log-normal distribution of fecal coliform (FC) concentration.

associations may be used to predict FIB from the values of the predictors alone.

Predictors may be drawn both from observations of water bodies and from other environmental conditions mechanistically linked with FIB loading and survival. The nature of the data available for each predictor affects the predictive scope of the model. Water quality characteristics are widely and effectively used to predict FIB at unobserved times for specific locations, such as particular beaches.[23,26−28] However, these variables typically require active data collection and physical access to the water body, limiting the scope of FIB prediction to the discrete locations and times that the predictors can be measured. Conversely, predictors with spatially or temporally continuous data coverage, such as those derived from meteorological and remote sensing (e.g., land use/land cover (LULC)) sources, can enable FIB prediction throughout the study domain.[29]

Spatiotemporal geostatistics provides a complementary approach that makes use of the spatial and temporal autocorrelation present in observed FIB concentrations to interpolate to unobserved locations and times.[25,30] Correlation between individual observations is liable to arise due to the structure of typical FIB monitoring, which entails repeatedly sampling hydrologically related locations. In geostatistics, a covariance model is estimated from the data to describe the decay in FIB autocorrelation over space and time, while simple empirical models typically treat each observation as independent. A significant advantage of geostatistics lies in the potential to directly consider spatiotemporal autocorrelation, which shifts correlated observations from a liability, capable of introducing bias, to a source of additional information for improving predictions.[31]

The geostatistical approach permits one to incorporate spatiotemporal correlation into a wide range of predictive modeling techniques by centering the data about an offset and modeling the residual covariance. The offset may be as simple as the mean of the data or predictions from simple empirical models, but several recent studies illustrate the flexibility of the approach by integrating spatiotemporal geostatistics and nonlinear land use regression (LUR) models to improve prediction of several water and air quality characteristics.[32−34] The geostatistical framework also provides a convenient means of incorporating physically meaningful processes into prediction through the choice of distance metric used in spatial covariance calculations. The ongoing development of permissible stream distance metrics with various flow-weighting schemes holds particular relevance for water quality prediction.[30,35−39]

DOI: 10.1021/acs.est.8b01178
Environ. Sci. Technol. 2018, 52, 7775−7784

In this study, we develop geostatistical models to expand the scope of FIB monitoring in a small watershed beyond discrete sample collection to assess microbial water quality throughout the stream network. Prediction at unmonitored locations and times is accomplished using readily available meteorological and LULC predictors. We compare the effects of different covariance model structures on predictive performance, including choice of distance metric, use of flow-weighting, and consideration of temporal autocorrelation. To demonstrate opportunities for enhancing monitoring and informing management, we map daily FIB concentrations and probabilistically identify locations with impaired water quality. Finally, we explore implications for setting efficient sampling priorities to support comprehensive monitoring of stream networks.

METHODS

Study Area. The B. Jordan Everett Dam and Lake was completed in 1982 to provide flood control and water supply in the Cape Fear River basin.[40] The Jordan Lake watershed spans ten counties in central North Carolina and serves as a water supply to eight municipal authorities in Chatham, Durham, Orange, and Wake counties, with a total allocation of 63 megagallons per day.[41] We studied the near-upstream Jordan Lake watershed (Figure 1), which includes portions of the Research Triangle Region and is characterized by rapid yet low-density land development at a rate exceeding population growth.[42]

Water Quality Assessment. Samples were collected biweekly between April 2010 and March 2011 for a total of 301 samples from 15 locations. We collected an additional 135 samples during storm events, wherein each site was sampled four times at predetermined intervals, as previously described.[11] FC were enumerated following standard membrane filtration methods.[43] We obtained 240 additional water quality observations for the years 2010 and 2011 from the EPA STORET online database for eight sites in the watershed, four colocated with our study sites, for a total of 676 FC observations (Figure 1).[44]

Meteorological Data. Records from the National Oceanic and Atmospheric (NOAA) U.S. Climate Reference Network (USCRN) Durham Station were used to assess the meteorological conditions of the watershed during the study time frame. Hourly records were obtained from the online National Climatic Data Center (now the National Centers for Environmental Information) for average surface temperature, incident solar radiation, and precipitation (Figure 1).[45] Recent precipitation ("new rain") was represented as the sum of precipitation (in mm) in the 48 h preceding each sample; similarly, precipitation further removed in time ("old rain") was assigned the sum of precipitation occurring between 48 and 168 h prior.[25] We used the mean incident solar radiation in the 4 h preceding each sampling time as the solar radiation input variable.

Stream Network Processing. A flow-connected, digital representation of the Jordan Lake watershed stream network was constructed in ESRI ArcMap 10.2 (Environmental Systems Research Institute, Redlands, CA, USA) using the ArcHydro toolbox and a digital elevation model (DEM) at 20 ft resolution from NC Department of Transportation (NCDOT).[46] We defined the stream network as contiguous cells with flow accumulation exceeding 30 000 to produce a network of adequate complexity without crowding by trivial tributaries. The stream network was converted to a Spatial Stream Network (SSN) topological data model object with the STARS toolbox in ArcGIS 10.2.[47] Inconsistencies in flow direction and stream convergence were manually corrected as necessary to meet the SSN model requirements. Downstream flow connection was represented using an additive step function derived from the catchment area of each stream segment (see Supporting Information).[37,47,48]

Upstream Watershed Delineation. We define the land area contributing runoff to the stream network upstream of a particular point on the network as the *upstream watershed* of that point. Flow-connected points are permitted overlapping upstream watersheds to capture the total land area contributing to each location. We implemented the *TopoToolbox-2.0.1-r* set of functions in MATLAB R2013a (The MathWorks, Inc., Natick, MA, USA) to delineate upstream watersheds for each sampling site and prediction location from NCDOT DEMS resampled at 30 m resolution.[49]

Land Cover Determination. LULC and percent impervious surface rasters were obtained for the year 2011 from the National Land Cover Database at 30 m resolution.[50] The percentage of watershed area comprising each land cover class was calculated in MATLAB by dividing the number of cells of each land cover class by the total number of cells in the watershed. To account for the range of development intensities, urbanizing land uses were represented as percent impervious surface. The mean watershed percent impervious surface was calculated by averaging the percent impervious surface value across all the cells in the watershed (Figure 1).

Geostatistical Model Fitting. All statistical analyses were performed in R 3.2.2 (R Foundation for Statistical Computing, Vienna, Austria).[51] Treating the natural logarithm transformed FC concentration data as the response variable, we assume a Gaussian geostatistical model:

$$\underset{n\times 1}{\ln(\mathbf{FC}(\boldsymbol{s},\boldsymbol{t}))} = \underset{n\times 1}{\boldsymbol{Y}(\boldsymbol{s},\boldsymbol{t})} = \underset{n\times p}{\boldsymbol{A}(\boldsymbol{s},\boldsymbol{t})}\ \underset{p\times 1}{\boldsymbol{\beta}} + \underset{n\times 1}{\boldsymbol{Z}(\boldsymbol{s},\boldsymbol{t})} \quad (1)$$

where the mean function ($\boldsymbol{A}(\boldsymbol{s},\boldsymbol{t})\boldsymbol{\beta}$) is a function of spatial coordinate matrix ($\boldsymbol{s}$) and time vector ($\boldsymbol{t}$), with the matrix of predictor variables ($\boldsymbol{A}(\boldsymbol{s},\boldsymbol{t})$) and coefficients vector ($\boldsymbol{\beta}$).[52] The error function ($\boldsymbol{Z}(\boldsymbol{s},\boldsymbol{t})$) is also a function of $\boldsymbol{s}$ and $\boldsymbol{t}$, comprising the variance explained by spatiotemporal autocorrelation in the data (the correlated error) and the variance unexplained by the model (the nugget). We considered different definitions of the error function ($\boldsymbol{Z}(\boldsymbol{s},\boldsymbol{t})$) to obtain five geostatistical models for comparison: an ordinary least-squares (OLS) model assuming fully uncorrelated error, a Euclidean spatial ("space-only") model, a stream distance spatial ("stream distance") model, a flow-weighted stream distance spatial ("flow-weighted") model, and a Euclidean separable spatiotemporal ("space/time") model.

We fit three time-indifferent geostatistical models to the observed FC concentrations using the function *glmssn*() from the SSN package.[37,48] By ignoring time, these models treat all observations as if they were collected simultaneously and reveal only the autocorrelation between locations that persists across sampling times. The flow-weighted model features an error function defined by a multistructure spatial covariance model incorporating a flow-weighted exponential stream distance model, an exponential Euclidean model, and a nugget. The flow-weighted stream distance component accounts for spatial autocorrelation between flow-connected locations with distance measured along a stream network, estimated using a moving average function that begins at some location and is

DOI: 10.1021/acs.est.8b01178
Environ. Sci. Technol. 2018, 52, 7775−7784

nonzero only as it moves upstream.[37] The Euclidean component accounts for spatial autocorrelation in the Euclidean distance between points, and the nugget accounts for uncorrelated error and ensures a positive definite covariance matrix. The three-structure spatial covariance model ($K_Z(s_i,s_j)$) for the spatially correlated error function ($\boldsymbol{Z}(\boldsymbol{s})$) is defined as

$$K_Z(s_i, s_j) = \sigma_f^2 C_f(s_i, s_j) + \sigma_e^2 C_e(s_i, s_j) + \sigma_n^2 \mathbb{1}\{s_i = s_j\} \quad (2)$$

where σ_f^2, σ_e^2, and σ_n^2 are the partial sills for the flow-weighted stream distance, Euclidean, and nugget components, respectively. Each partial sill is the variance accounted for by the corresponding error function component, such that the sum of the partial sills equals the error function variance (σ^2), which is the total variance not explained by the mean function. The correlation model for the flow-weighted stream distance structure ($C_f(s_i,s_j)$) is

$$C_f(s_i, s_j) = \begin{cases} \pi_{i,j}\exp(-3r/\alpha_f) & \text{if } s_i \text{ and } s_j \text{ are flow connected} \\ 0 & \text{if } s_i \text{ and } s_j \text{ are not flow connected} \end{cases} \quad (3)$$

for stream distance (r) between the upstream point (s_i) and downstream point (s_j) and with flow weights $\left(\pi_{i,j} = \sqrt{\frac{\Omega(s_i)}{\Omega(s_j)}}\right)$, where $\Omega(\cdot)$ is the additive function defined for the underlying stream segments.[30,37] Similarly,

$$C_e(s_i, s_j) = \exp(-3d/\alpha_e) \quad (4)$$

is the correlation model for the Euclidean structure, where $d = \|s_i - s_j\|$, the Euclidean distance metric.[37,48] The range parameters (α_f and α_e) are the distances between s_i and s_j at which the partial covariance between the two points decays to approximately 5% of the partial sill corresponding to that covariance structure.

We used maximum likelihood to estimate the parameters ($\boldsymbol{\beta}$, σ_f^2, σ_e^2, σ_n^2, α_f, and α_e) for the full model, which included all the potential meteorological and LULC covariates in the design matrix ($\boldsymbol{A}(\boldsymbol{s},\boldsymbol{t})$).[53] Predictors were standardized to improve interpretability by subtracting the sample mean of each covariate and dividing by the standard deviation.[54] The final model was obtained by removing covariates through a backward elimination procedure to minimize the Akaike Information Criterion (AIC), a function of the likelihood penalized by the number of parameters estimated.[55] The remaining four models were fit using the same set of predictors to aid comparison between models.

We fit a stream distance spatial model without flow-weighting to permit spatial autocorrelation along the stream network between points that are not flow connected. We modify (2) to obtain

$$K_Z(s_i, s_j) = \sigma_r^2 C_r(s_i, s_j) + \sigma_e^2 C_e(s_i, s_j) + \sigma_n^2 \mathbb{1}\{s_i = s_j\} \quad (5)$$

with stream distance partial sill (σ_r^2) and stream distance correlation model ($C_r(s_i,s_j)$), which is equivalent to (4), substituting the stream distance (r) for the Euclidean distance (d). The stream distance covariance structure in (5) is dropped to obtain the third spatial model with the Euclidean covariance structure and nugget only. The stream distance and Euclidean space-only models were fit using maximum likelihood estimation implemented in the *glmssn*() function in the same manner as the flow-weighted model.

To account for temporal autocorrelation in the error function ($\boldsymbol{Z}(\boldsymbol{s},\boldsymbol{t})$) from (1), we modify the error function in (2) to obtain

$$K_Z((s_i, s_j), (t_i, t_j)) = \sigma_e^2 C_e((s_i, s_j), (t_i, t_j)) + \sigma_n^2 \mathbb{1}\{s_i = s_j, t_i = t_j\} \quad (6)$$

where $C_e((s_i,s_j),(t_i,t_j))$ is the space/time separable exponential correlation model

$$C_e((s_i, s_j), (t_i, t_j)) = \exp\left(-\frac{3\|s_i - s_j\|}{\alpha_e}\right)\exp\left(-\frac{3|t_i - t_j|}{\alpha_t}\right) \quad (7)$$

with Euclidean spatial range parameter (α_e) and temporal range (α_t).[56] The Euclidean space/time model parameters ($\boldsymbol{\beta}$, σ_n^2, σ_e^2, α_e, and α_t) were obtained using maximum likelihood estimation with profiling of the mean function parameters ($\boldsymbol{\beta}$) (Supporting Information).[53] We did not consider temporal covariance for models implementing stream distance metrics due to limitations in the software package.[48]

We used leave-one-out cross validation (LOOCV) to compare the predictive performance of the five models (Supporting Information).[32] Prediction accuracy was assessed through the root-mean-square error (RMSE), and the proportion of variance in the data explained by each model was represented by the corrected prediction R^2. Validation statistics are calculated as

$$\text{RMSE} = \left(\frac{1}{n}\hat{\boldsymbol{\epsilon}}_p^T\hat{\boldsymbol{\epsilon}}_p\right)^{1/2}$$

$$R^2 = \frac{\hat{\boldsymbol{\epsilon}}_0^T\hat{\boldsymbol{\epsilon}}_0 - \hat{\boldsymbol{\epsilon}}_p^T\hat{\boldsymbol{\epsilon}}_p}{\hat{\boldsymbol{\epsilon}}_0^T\hat{\boldsymbol{\epsilon}}_0} \quad (8)$$

for the vectors of LOOCV prediction residuals ($\hat{\boldsymbol{\epsilon}}_p = \boldsymbol{Y} - \hat{\boldsymbol{Y}}$) and mean residuals $\left(\hat{\boldsymbol{\epsilon}}_{\boldsymbol{p}} = \boldsymbol{Y} - \left(\frac{\sum_{i=1}^n y_i}{n}\right)\right)$, where $\boldsymbol{Y}$ and $\hat{\boldsymbol{Y}}$ are the vectors of observations and predictions, respectively.

Prediction at Unmonitored Locations and Times. We predicted FC concentrations at 580 spatial locations arranged equidistant along the stream network, including the 19 study sampling sites.[52] Predictions were made using the meteorological covariate values at 11:00 a.m. on each day of the study period. The best performing geostatistical model by lowest AIC was used to implement universal kriging, where the prediction mean ($\hat{y}_k$) at location (s_k) and time (t_k) is

$$\hat{y}_k = \boldsymbol{a}_k^T\hat{\boldsymbol{\beta}} + \boldsymbol{\Sigma}_{kh}\boldsymbol{\Sigma}_{hh}^{-1}(\boldsymbol{Y} - \boldsymbol{A}\hat{\boldsymbol{\beta}}) \quad (9)$$

for the vector of covariate values ($\boldsymbol{a}_k$), observation covariance matrix ($\boldsymbol{\Sigma}_{hh}$), and cross-covariance vector ($\boldsymbol{\Sigma}_{kh}$).[52] The prediction standard error is approximated as

$$\hat{\sigma}_k = \sqrt{\hat{\sigma}^2 - \boldsymbol{\Sigma}_{\boldsymbol{kh}}\boldsymbol{\Sigma}_{\boldsymbol{hh}}^{-1}\boldsymbol{\Sigma}_{\boldsymbol{kh}}^T} \quad (10)$$

where $\hat{\sigma}^2$ is the estimated model variance (Supporting Information).

Assessing Watershed Impairment. We used an impairment metric developed by Akita et al. to classify the proportion of river miles on each study day predicted to be impaired, unimpaired, and unassessed, based on the NC surface water

DOI: 10.1021/acs.est.8b01178
Environ. Sci. Technol. 2018, 52, 7775−7784

Table 1. Comparison of Model Performance and Proportion of Variance Explained by Geostatistical Model Components

		performance metrics			proportion of variance explained		
						error function	
model	covariance structure	AIC	RMSE[a] [ln(cfu)]	R^2[a]	mean function	correlated error proportion	unexplained variance (nugget) proportion
OLS	nugget	2214	1.21	0.59	0.59		0.41
space-only	Euclidean + nugget	2187	1.19	0.61	0.59	0.03	0.38
stream distance	stream distance + Euclidean + nugget	2191	1.19	0.61	0.59	0.03	0.38
flow-weighted	flow-weighted stream distance + Euclidean + nugget	2191	1.19	0.61	0.59	0.03	0.38
space/time	Euclidean + nugget	2090	1.02	0.71	0.59	0.34	0.07

[a]Calculated from LOOCV prediction residuals.

Table 2. Error Function Parameter Estimates

	unexplained variance (nugget)	Euclidean covariance			stream distance covariance	
model	partial sill [ln(cfu)^2]	partial sill [ln(cfu)^2]	spatial range [km]	temporal range [days]	partial sill [ln(cfu)^2]	spatial range [km]
OLS	1.48					
space-only	1.36	0.112	8.8			
stream distance	1.36	0.112	8.9		3.4×10^{-4}	10.4
flow-weighted	1.36	0.098	9.3		0.012	22.7
space/time	0.24	1.23	12.8	2.1		

quality standard for fecal coliform concentration of 200 cfu/100 mL.[31,39,57,58] The probability that each prediction point exceeded the state standard was calculated using the kriging prediction mean and standard error. Predictions with ≥0.9 probability of exceeding the state standard were categorized as impaired; those with ≤0.1 probability of exceeding the standard were categorized as unimpaired, and predictions with probabilities of exceeding the standard >0.1 but <0.9 were considered unassessed. Additionally, any points with >0.5 probability of exceeding the standard were considered more likely than not to be impaired.

RESULTS AND DISCUSSION

Geostatistical Model Comparison. We fit an OLS model, assuming uncorrelated error, and four geostatistical models, distinguished by four different covariance models for the error function, to FC concentration data. Table 1 compares the performance of the five models, which were assessed foremost by minimizing AIC, followed by RMSE and corrected prediction R^2. The OLS model and the three spatial models performed similarly, with the OLS model faring slightly worse by all three metrics and the Euclidean space-only model performing slightly better by AIC. The three spatial models all estimated the same proportion of spatial autocorrelation (3% of the total variance) regardless of covariance model structure. Incorporating temporal autocorrelation greatly improved performance, substantially reducing AIC and RMSE and allowing the space/time model to explain over 70% of the variance in FC concentration. The mean function explained the greatest variance portion (59%) in all four geostatistical models; the OLS model also explained 59% of the total variance. The correlated error component of the space/time model accounted for 34% of the total variance, far exceeding the 3% correlated error in the spatial models. RSME and R^2 values for space/time model predictions at individual sampling sites ranged from 0.61 to 1.48 ln(cfu)/100 mL and from 0.42 to 0.88, respectively (Table S4).

Effects of Stream Distance and Spatiotemporal Autocorrelation: Error Function Models. Compared with the OLS model assuming uncorrelated error, we observed a strong improvement in model performance by considering temporal autocorrelation but little improvement when modeling the error function using only spatial autocorrelation (Table 2). Incorporating a stream distance metric had no effect on model performance, as Euclidean distance-based autocorrelation dominated the spatially correlated error. The longest spatial range was associated with the flow-weighted stream distance component, but the small partial sill suggests limited impact of stream processes in driving FC concentrations, further reflected in the negligible partial sill and reduced spatial range of the stream distance model without flow-weighting.

Scale may be an important factor in the relative importance of land and stream-based processes driving microbial contamination; overland processes appear to dominate in-stream processes in our small watershed, with sampling locations at most 20 km apart. A recent study conducted on a similarly small watershed likewise realized only minor performance gains by modeling correlated error using a flow-weighted stream distance metric, despite observing substantial spatial autocorrelation.[59] In contrast, other studies conducted on whole river basins found the stream distance metric (with various flow-weighting schemes) improved FIB estimation, suggesting that in-stream effects may grow dominant at larger scales.[30,39] Larger spatial scales generally increase the number of flow-connected sampling locations analyzed, which may lead to performance gains from flow-weighted and stream distance metrics.[60] Several studies predicting other physiochemical characteristics in streams obtained mixed results regarding the relative performance of Euclidean versus (flow-weighted) stream distance metrics.[35,57,61−63] The appropriate distance metric for modeling a particular water quality characteristic is dependent on several interacting factors, including the underlying processes driving the characteristic, the spatial scale of the analysis, and the distribution of sampling locations on the network.[64]

DOI: 10.1021/acs.est.8b01178
Environ. Sci. Technol. 2018, 52, 7775−7784

When time was included, the amount of uncorrelated error was substantially decreased, though temporal autocorrelation fully decayed in 2 days. In contrast to the spatial models, the space/time model only estimates spatial autocorrelation for observations made within this short temporal range, revealing much stronger spatial patterns. The short temporal range, increased spatial range, and large partial sill suggest that localized microbial water quality is dependent on broader environmental conditions that are subject to substantial temporal variability. This is in keeping with previous research at freshwater beaches, in which the day of sampling explained the largest portion of FIB concentration variance between multiple beaches.[19] As such, the space/time model may be useful for predicting water quality at unmonitored locations when microbial concentrations are known elsewhere but is limited for prediction at unmonitored times.

Effects of Land Cover and Meteorology: Mean Function Models. We used the standardized predictor variables to specify a full mean function for the flow-weighted model (Table S3). The model with the lowest AIC following backward elimination retained the following predictors: percent forested upstream watershed area, percent agricultural upstream watershed area, hourly average surface temperature, precipitation in the preceding 2 days, precipitation in the preceding 7 days (excluding the previous 2 days), and the interaction between the two precipitation terms. The other four models were fit to the same set of predictors. The parameter estimates differed slightly between the five models due to the influence of covariance structure (Table S2), but the mean function for all five models accounted for the same proportion of the total variance in the data (Table 1).

The direction of effect estimates (Figure 2) largely coincided with our expectations. Increasing forest cover was protective against microbial pollution,[11,14,65,66] while antecedent rainfall and warmer temperatures were associated with increased microbial concentrations.[11,13,16,23,25,67] Precipitation in the preceding 2 days was associated with the largest increase in FC concentration. Agricultural land use also exhibited a strong positive relationship with FC, though it was the least precise parameter estimate and previous studies report conflicting effects of agriculture on FIB.[11,66,68] This uncertainty could relate to the geographic distribution of agricultural land on the periphery of the study area: although many sites had agricultural lands upstream, the watersheds generally transitioned to other land uses nearer the sites.

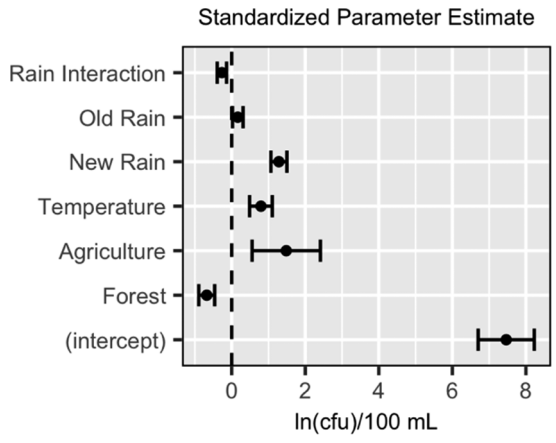

Figure 2. Mean function GLS parameter estimates (points) and 95% confidence intervals (bars) for the space/time model. Estimates are for standardized (mean-centered, standard deviation-scaled) input variables and represent the expected change in ln(FC) concentration for a 1 standard deviation increase in the input variable with all other variables held constant. Note that the three rain terms are related through the interaction and cannot be interpreted in isolation (Supporting Information). The intercept corresponds to the expected ln(FC) concentration when all other predictors equal their respective means.

Despite previous studies suggesting urbanization increases microbial pollution, we did not observe a significant association between increasing impervious surfaces and FC concentration.[11,14,66,69] Though urbanized land was common, most watersheds had low impervious surface percentages, reflecting low-intensity development with potentially diffuse impacts on FC loading. We also failed to detect a significant effect of solar radiation, which is known to inactivate microbes in the environment.[65,67,70−72] This may be due in part to the spatial coarseness of the solar radiation measurement, for which a single value measured at the NOAA Durham station was used for all samples collected at a given time. Site-specific topography and canopy cover could have substantially altered the amount of solar radiation reaching the water. To address these limitations, future applications may consider model-based estimation of solar radiation, which has been used effectively in mechanistic FIB models.[28,73−75]

The models presented here provide nuanced estimates of the overall effects of precipitation by considering the interaction between the two precipitation time frames. More recent precipitation has a stronger effect on microbial concentration than precipitation further removed in time, but the negative interaction estimate suggests that past precipitation mitigates the impact of more recent precipitation (Supporting Information). In systems where FC sources accumulate on land before precipitation flushes contamination into water bodies, it follows that past precipitation reduces the stock of contamination available for subsequent rain to wash into the stream. Precipitation intensity may also act as an important driver of contamination in some systems, although it did not appreciably affect the predictive performance of the models presented in this paper (data not shown).

Although likely similar to many other mixed-use watersheds, the associations between FC and the predictors considered in this study should be generalized with caution. The study area comprised a small watershed with limited LULC composition, the effects of which were derived essentially from 19 observations for each LULC class (corresponding to the 19 sampling sites). As with the covariance components, scale likely also affects the magnitude of predictor effects. The pronounced sensitivity to precipitation might be tempered in larger systems featuring spatially heterogeneous meteorological conditions and a wider range of LULC characteristics. Furthermore, we might expect associations with meteorology to differ in systems dominated by sources with distinctive loading dynamics, such as agricultural watersheds receiving intermittent manure applications.

Space/Time Prediction of Microbial Water Quality. The space/time geostatistical model was chosen to predict FC concentrations at unmonitored locations and times. We predicted universal kriging means and standard errors at each prediction location at 11 a.m. for each of the 365 days between April 1, 2010 and March 31, 2011 and calculated the probability each prediction exceeded the NC standard of 200

DOI: 10.1021/acs.est.8b01178
Environ. Sci. Technol. 2018, 52, 7775−7784

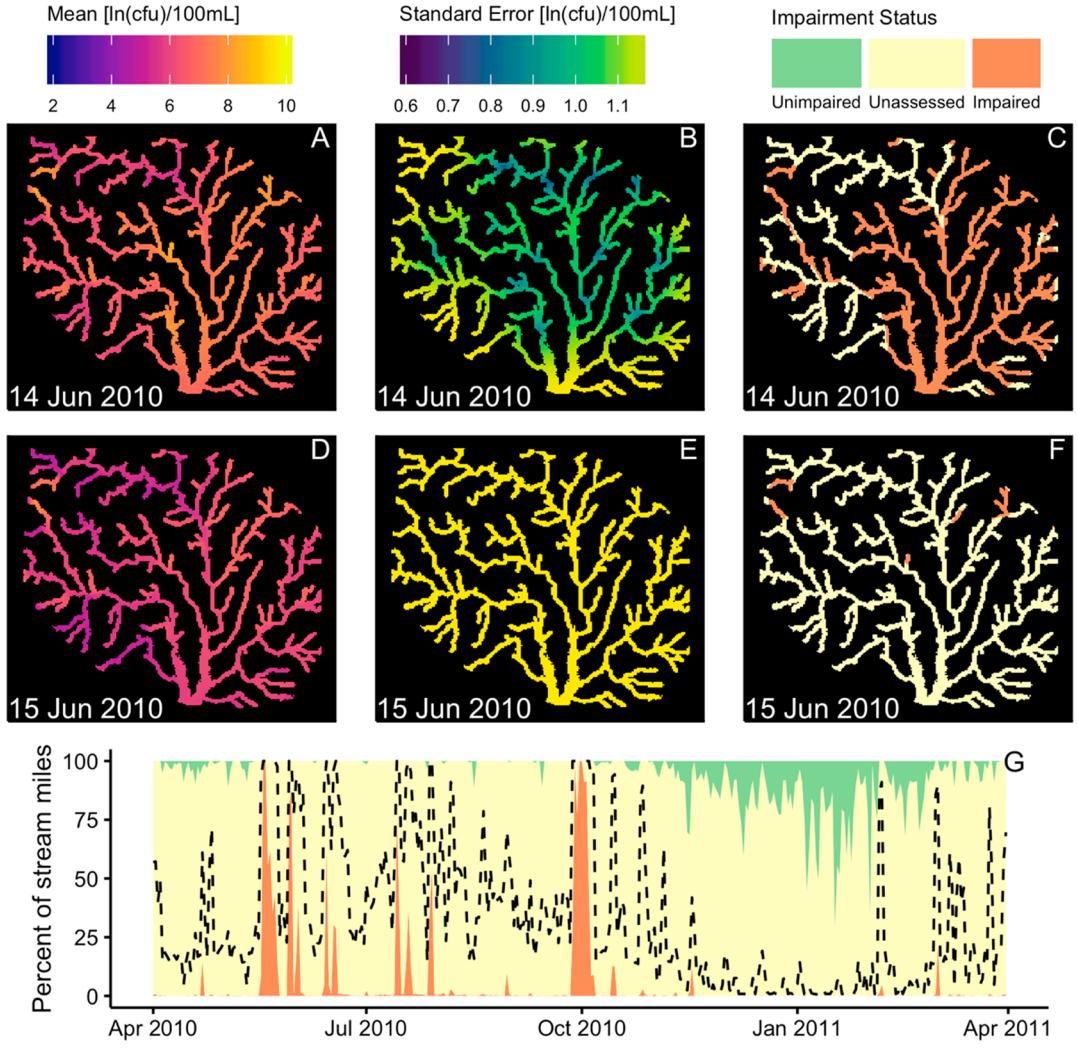

Figure 3. Predicted spatial and temporal trends in microbial water quality. The top two rows (panels A–F) map the prediction means (panels A and D), standard errors (panels B and E), and impairment status (panels C and F) for the whole study area on two consecutive days. The bottom row (panel G) is the percentage of stream miles assigned each impairment status by day for the entire one-year study period, using the same scale as the impairment status maps; the dashed line represents the percentage of stream miles more likely impaired than not. Water samples were collected for the first day, which is reflected in the lower standard errors (panel B) compared with the following day (panel E), for which no sample data are available. Areas assigned an impaired status on the first day (panel C) largely correspond to the areas of reduced standard error arising from the observational data (panel B).

cfu/100 mL, from which a corresponding impairment status was assigned. Figure 3 illustrates the spatial and temporal trends in prediction mean, standard error, and impairment status. Prediction error was lower on days FC were measured (Figure 3B), but the short temporal range largely prevented observational data from affecting predictions on consecutive days (Figure 3E). Predictions outside the temporal range were made entirely on the basis of the mean function, which can be observed in the flattening of localized prediction means between days with and without sample data (Figure 3A,D).

Mean FC concentrations exceeding the standard were predicted on every day of the study; on 36 days (10% of study period), more than 90% of stream miles had predicted FC means above the standard. When impairment status was assigned only to predictions with a high probability (≥90%) of being above or below the state standard, some portion of the watershed was considered impaired on 209 days (57%), while unimpaired stream miles were predicted on 190 days (52%). We observed no strong spatial patterns of impairment; rather, impairment tended to be event driven, wherein large portions of the watershed briefly became impaired before a relatively rapid return to a generally unassessed state (Figure 3G). While unimpairment likewise displayed no strong spatial pattern, the temporal trends for unimpaired stream miles appeared more seasonally driven, with notable background levels of unimpaired stream miles during the winter months. Conversely, relatively few stream miles were considered unimpaired during months in which impairment events are more common, even when no impairment event was ongoing; in such cases, the majority of the watershed was considered unassessed.

Role of Predictive Models and Observational Data in Assessing Watershed Impairment. Our space/time model predicted that the Jordan Lake near-upstream watershed frequently suffered from unsafe levels of microbial contamination. However, despite 33% of all prediction means exceeding the state standard, only 5% of predictions could be confidently considered impaired, and only 6% were confidently assessed as unimpaired. The other 89% of

DOI: 10.1021/acs.est.8b01178
Environ. Sci. Technol. 2018, 52, 7775–7784

predictions were unassessed, meaning we could not determine whether FC concentrations fell above or below the NC standard after accounting for prediction uncertainty. Access to water sample data on the day of prediction was strongly associated with an increased ability to assign impairment status. Under a simple linear regression, any observation of FC on a given day was associated with a 20% reduction ($p < 0.001$) in unassessed stream miles.

Because impairment appears largely event-driven, increases in related meteorological variables, particularly precipitation, produced elevated mean FC predictions. However, the high temporal variability and low temporal autocorrelation range of FC concentrations limited the ability of models alone to predict impairment status with high confidence. Access to recent monitoring data, however, reduced prediction uncertainty sufficiently to confidently assign impairment status to larger portions of the stream network. While a recent study in a similar watershed observed clear spatial patterns in FIB, they did not translate into the substantial reductions in prediction error necessary to confidently assess impairment status.[59] Their samples were collected monthly, without intentional storm sampling or considering temporal autocorrelation, which suggests spatial relationships may impact background FIB concentrations, only to be drowned out by events driving brief, widespread impairment. This dynamic suggests frequent, sample-based monitoring remains necessary to confidently assess the safety and legal status of a water body. The implementation of spatiotemporal predictive models may reduce the number of concurrent sampling locations required to adequately assess water quality throughout a stream network, providing the means to increase sampling frequency without increasing monitoring expenses.

In developing geostatistical models that consider the spatiotemporal patterns and environmental drivers of microbial water quality impairment, we identified clearly dominant factors in each structural model component that together largely explain observed FC concentrations and enable their prediction. Precipitation dominated in the model component that predicts FC directly, while temporal patterns dominated spatial patterns in the component that contributes indirectly to prediction by considering autocorrelation in the outcome. Rather than orienting monitoring activities around specific locations of heightened concern, the dominance of precipitation and temporal effects suggests a monitoring strategy that targets sampling according to temporal criteria, employing frequent sampling to better capture diverse meteorological conditions driving impairment events. Because we constructed the model using remotely sensed and continuously reported predictors and we jointly estimated the different model component parameters using likelihood-based methods, others may apply the model to geographically sparse monitoring data to assess microbial water quality impairment throughout stream networks without the need for additional specialized measurements or knowledge. Environmental managers, regulators, and researchers can implement our model to inform management decisions, target remediation efforts, and issue timely warnings for the protection of public health.

■ ASSOCIATED CONTENT

Supporting Information

The Supporting Information is available free of charge on the ACS Publications website at DOI: 10.1021/acs.est.8b01178.

Profiling for maximum likelihood estimation; universal kriging prediction error approximation; additive function values for flow-weighting; exploratory analysis of input variables; visual interpretation of error function; mean function parameter estimates; derivation of precipitation interaction effects; prediction at individual sampling sites; animated maps of daily watershed predictions (PDF)

■ AUTHOR INFORMATION

Corresponding Author

*E-mail: jill.stewart@unc.edu; phone: (919) 966-7553.

ORCID

David A. Holcomb: 0000-0003-4055-7164

Jill R. Stewart: 0000-0002-3474-5233

Notes

The authors declare no competing financial interest.

■ ACKNOWLEDGMENTS

This work was supported in part by the Water Resources Research Institute of the University of North Carolina, project number 70252. We are grateful to Prahlad Jat for assisting with the stream network analysis and display.

■ REFERENCES

(1) Dadswell, J. V. Microbiological Quality of Coastal Waters and Its Health Effects. *Int. J. Environ. Health Res.* **1993**, *3* (1), 32−46.

(2) Byappanahalli, M. N.; Nevers, M. B.; Korajkic, A.; Staley, Z. R.; Harwood, V. J. Enterococci in the Environment. *Microbiol. Mol. Biol. Rev.* **2012**, *76* (4), 685−706.

(3) Dorevitch, S.; Pratap, P.; Wroblewski, M.; Hryhorczuk, D. O.; Li, H.; Liu, L. C.; Scheff, P. A. Health Risks of Limited-Contact Water Recreation. *Environ. Health Perspect.* **2011**, *120* (2), 192−197.

(4) Soller, J. A.; Schoen, M. E.; Bartrand, T.; Ravenscroft, J. E.; Ashbolt, N. J. Estimated Human Health Risks from Exposure to Recreational Waters Impacted by Human and Non-Human Sources of Faecal Contamination. *Water Res.* **2010**, *44* (16), 4674−4691.

(5) Marion, J. W.; Lee, J.; Lemeshow, S.; Buckley, T. J. Association of Gastrointestinal Illness and Recreational Water Exposure at an Inland U.S. Beach. *Water Res.* **2010**, *44* (16), 4796−4804.

(6) Brown, J. M.; Proum, S.; Sobsey, M. D. Escherichia Coli in Household Drinking Water and Diarrheal Disease Risk: Evidence from Cambodia. *Water Sci. Technol.* **2008**, *58* (4), 757.

(7) Wade, T. J.; Pai, N.; Eisenberg, J. N. S.; Colford, J. M. Do U.S. Environmental Protection Agency Water Quality Guidelines for Recreational Waters Prevent Gastrointestinal Illness? A Systematic Review and Meta-Analysis. *Environ. Health Perspect.* **2003**, *111* (8), 1102−1109.

(8) Colford, J. M.; Wade, T. J.; Schiff, K. C.; Wright, C. C.; Griffith, J. F.; Sandhu, S. K.; Burns, S.; Sobsey, M.; Lovelace, G.; Weisberg, S. B. Water Quality Indicators and the Risk of Illness at Beaches With Nonpoint Sources of Fecal Contamination. *Epidemiology* **2007**, *18* (1), 27−35.

(9) *Federal Water Pollution Control Act*; 33 U.S.C. §§1251−1387; 1972; https://www3.epa.gov/npdes/pubs/cwatxt.txt.

(10) USEPA. *National Summary of State Information*; http://iaspub.epa.gov/waters10/attains_nation_cy.control (accessed Sep 25, 2015).

(11) Rowny, J. G.; Stewart, J. R. Characterization of Nonpoint Source Microbial Contamination in an Urbanizing Watershed Serving as a Municipal Water Supply. *Water Res.* **2012**, *46* (18), 6143−6153.

(12) Mallin, M. A.; Johnson, V. L.; Ensign, S. H. Comparative Impacts of Stormwater Runoff on Water Quality of an Urban, a Suburban, and a Rural Stream. *Environ. Monit. Assess.* **2009**, *159* (1−4), 475−491.

DOI: 10.1021/acs.est.8b01178
Environ. Sci. Technol. 2018, 52, 7775−7784

(13) Coulliette, A. D.; Noble, R. T. Impacts of Rainfall on the Water Quality of the Newport River Estuary (Eastern North Carolina, USA). *J. Water Health* **2008**, *06* (4), 473.
(14) DiDonato, G. T.; Stewart, J. R.; Sanger, D. M.; Robinson, B. J.; Thompson, B. C.; Holland, A. F.; Van Dolah, R. F. Effects of Changing Land Use on the Microbial Water Quality of Tidal Creeks. *Mar. Pollut. Bull.* **2009**, *58* (1), 97−106.
(15) Stumpf, C. H.; Piehler, M. F.; Thompson, S.; Noble, R. T. Loading of Fecal Indicator Bacteria in North Carolina Tidal Creek Headwaters: Hydrographic Patterns and Terrestrial Runoff Relationships. *Water Res.* **2010**, *44* (16), 4704−4715.
(16) Liao, H.; Krometis, L.-A. H.; Cully Hession, W.; Benitez, R.; Sawyer, R.; Schaberg, E.; von Wagoner, E.; Badgley, B. D. Storm Loads of Culturable and Molecular Fecal Indicators in an Inland Urban Stream. *Sci. Total Environ.* **2015**, *530−531*, 347−356.
(17) Leecaster, M. K.; Weisberg, S. B. Effect of Sampling Frequency on Shoreline Microbial Assessments. *Mar. Pollut. Bull.* **2001**, *42* (11), 1150−1154.
(18) Whitman, R. L.; Nevers, M. B. Escherichia Coli Sampling Reliability at a Frequently Closed Chicago Beach: Monitoring and Management Implications. *Environ. Sci. Technol.* **2004**, *38* (16), 4241−4246.
(19) Whitman, R. L.; Nevers, M. B. Summer E. Coli Patterns and Responses along 23 Chicago Beaches. *Environ. Sci. Technol.* **2008**, *42* (24), 9217−9224.
(20) USEPA. Predictive Tools for Beach Notification.; EPA-823-R-10-003; 2010; https://www.epa.gov/sites/production/files/2015-11/documents/predictive-tools-volume1.pdf.
(21) Nevers, M. B.; Whitman, R. L. Efficacy of Monitoring and Empirical Predictive Modeling at Improving Public Health Protection at Chicago Beaches. *Water Res.* **2011**, *45* (4), 1659−1668.
(22) Avila, R.; Horn, B.; Moriarty, E.; Hodson, R.; Moltchanova, E. Evaluating Statistical Model Performance in Water Quality Prediction. *J. Environ. Manage.* **2018**, *206*, 910−919.
(23) Gonzalez, R. a.; Conn, K. E.; Crosswell, J. R.; Noble, R. T. Application of Empirical Predictive Modeling Using Conventional and Alternative Fecal Indicator Bacteria in Eastern North Carolina Waters. *Water Res.* **2012**, *46* (18), 5871−5882.
(24) Farnham, D. J.; Lall, U. Predictive Statistical Models Linking Antecedent Meteorological Conditions and Waterway Bacterial Contamination in Urban Waterways. *Water Res.* **2015**, *76*, 143−159.
(25) Coulliette, A. D.; Money, E. S.; Serre, M. L.; Noble, R. T. Space/Time Analysis of Fecal Pollution and Rainfall in an Eastern North Carolina Estuary. *Environ. Sci. Technol.* **2009**, *43* (10), 3728−3735.
(26) Nevers, M. B.; Whitman, R. L. Nowcast Modeling of Escherichia Coli Concentrations at Multiple Urban Beaches of Southern Lake Michigan. *Water Res.* **2005**, *39* (20), 5250−5260.
(27) Eleria, A.; Vogel, R. M. Predicting Fecal Coliform Bacteria Levels in the Charles River, Massachusetts, USA. *J. Am. Water Resour. Assoc.* **2005**, *41* (5), 1195−1209.
(28) Safaie, A.; Wendzel, A.; Ge, Z.; Nevers, M. B.; Whitman, R. L.; Corsi, S. R.; Phanikumar, M. S. Comparative Evaluation of Statistical and Mechanistic Models of Escherichia Coli at Beaches in Southern Lake Michigan. *Environ. Sci. Technol.* **2016**, *50* (5), 2442−2449.
(29) Zhang, Z.; Deng, Z.; Rusch, K. A.; Walker, N. D. Modeling System for Predicting Enterococci Levels at Holly Beach. *Mar. Environ. Res.* **2015**, *109*, 140−147.
(30) Money, E. S.; Carter, G. P.; Serre, M. L. Modern Space/Time Geostatistics Using River Distances: Data Integration of Turbidity and E. Coli Measurements to Assess Fecal Contamination Along the Raritan River in New Jersey. *Environ. Sci. Technol.* **2009**, *43* (10), 3736−3742.
(31) Akita, Y.; Carter, G.; Serre, M. L. Spatiotemporal Nonattainment Assessment of Surface Water Tetrachloroethylene in New Jersey. *J. Environ. Qual.* **2007**, *36* (2), 508.
(32) Messier, K. P.; Kane, E.; Bolich, R.; Serre, M. L. Nitrate Variability in Groundwater of North Carolina Using Monitoring and Private Well Data Models. *Environ. Sci. Technol.* **2014**, *48* (18), 10804−10812.
(33) Messier, K. P.; Campbell, T.; Bradley, P. J.; Serre, M. L. Estimation of Groundwater Radon in North Carolina Using Land Use Regression and Bayesian Maximum Entropy. *Environ. Sci. Technol.* **2015**, *49* (16), 9817−9825.
(34) Reyes, J. M.; Serre, M. L. An LUR/BME Framework to Estimate PM2.5 Explained by on Road Mobile and Stationary Sources. *Environ. Sci. Technol.* **2014**, *48* (3), 1736−1744.
(35) Money, E.; Carter, G. P.; Serre, M. L. Using River Distances in the Space/Time Estimation of Dissolved Oxygen along Two Impaired River Networks in New Jersey. *Water Res.* **2009**, *43* (7), 1948−1958.
(36) Money, E. S.; Sackett, D. K.; Aday, D. D.; Serre, M. L. Using River Distance and Existing Hydrography Data Can Improve the Geostatistical Estimation of Fish Tissue Mercury at Unsampled Locations. *Environ. Sci. Technol.* **2011**, *45* (18), 7746−7753.
(37) Ver Hoef, J. M.; Peterson, E. E. A Moving Average Approach for Spatial Statistical Models of Stream Networks. *J. Am. Stat. Assoc.* **2010**, *105* (489), 6−18.
(38) Cressie, N.; Frey, J.; Harch, B.; Smith, M. Spatial Prediction on a River Network. *J. Agric. Biol. Environ. Stat.* **2006**, *11* (2), 127−150.
(39) Jat, P.; Serre, M. L. A Novel Geostatistical Approach Combining Euclidean and Gradual-Flow Covariance Models to Estimate Fecal Coliform along the Haw and Deep Rivers in North Carolina. *Stoch. Environ. Res. Risk Assess.* **2018**, DOI: 10.1007/s00477-018-1512-6.
(40) USACE. *B. Everett Jordan Dam and Lake Master Plan Update Draft Report*; United States Army Corps of Engineers: Wilmington, NC, 2007; ftp://ftp.chathamnc.org/Chatham_ConservationPlan_GIS/Plans_Policies_Ordinances/USACoE_Jordan%20Lake%20Master%20Plan%20Update.pdf.
(41) NCDENR. *Jordan Lake Current Allocations*; North Carolina Department of Environment and Natural Resources: Raleigh, NC; http://www.ncwater.org/?page=313 (accessed Sep 18, 2015).
(42) Hodges-Copple, J. An Overview of the Research Triangle Region of North Carolina; In *Presentations*, CAMPO Expert Panel, Raleigh, NC, November 2011; NC Capital Area Metropolitan Planning Organization: Raleigh, NC, 2011.
(43) APHA; AWWA; WEF. *Standard Methods for the Examination of Water and Wastewater*, 20th ed.; American Public Health Association, American Waterworks Association, Water Environment Federation: Washington, D.C, 1998.
(44) USEPA. *STORET Data Warehouse*; United States Environmental Protection Agency: Washington, DC; http://www.epa.gov/storet/dbtop.html (accessed Sep 10, 2013).
(45) Diamond, H. J.; Karl, T. R.; Palecki, M. A.; Baker, C. B.; Bell, J. E.; Leeper, R. D.; Easterling, D. R.; Lawrimore, J. H.; Meyers, T. P.; Helfert, M. R.; Goodge, G.; Thorne, P. W. U.S. Climate Reference Network after One Decade of Operations: Status and Assessment. *Bull. Am. Meteorol. Soc.* **2013**, *94* (4), 485−498.
(46) NCDOT. *Elevation/DEM20ft_DEM*; North Carolina Department of Transportation: Raleigh, NC, 2014. https://services.nconemap.gov/secure/rest/services/Elevation/DEM20ft_DEM/ImageServer.
(47) Peterson, E. E.; Ver Hoef, J. M. STARS: An ArcGIS Toolset Used to Calculate the Spatial Information Needed to Fit Spatial Statistical Models to Stream Network Data. *J. Stat. Softw.* **2014**, *56* (2), 1−17.
(48) Ver Hoef, J. M.; Peterson, E. E.; Clifford, D.; Shah, R. SSN: An R Package for Spatial Statistical Modeling on Stream Networks. *J. Stat. Softw.* **2014**, *56* (3), 1−45.
(49) Schwanghart, W.; Kuhn, N. J. TopoToolbox: A Set of Matlab Functions for Topographic Analysis. *Environ. Model. Softw.* **2010**, *25* (6), 770−781.
(50) Homer, C. G.; Dewitz, J. A.; Yang, L.; Jin, S.; Danielson, P.; Xian, G.; Coulston, J.; Herold, N. D.; Wickham, J. D.; Megown, K. Completion of the 2011 National Land Cover Database for the Conterminous United States-Representing a Decade of Land Cover

DOI: 10.1021/acs.est.8b01178
Environ. Sci. Technol. 2018, 52, 7775−7784

Change Information. *Photogramm. Eng. Remote Sensing* **2015**, *81* (5), 345−354.
(51) R Core Team. *R: A Language and Environment for Statistical Computing*; R Foundation for Statistical Computing: Vienna, Austria, 2017.
(52) Zimmerman, D. L.; Stein, M. Classical Geostatistical Methods. In *Handbook of Spatial Statistics*; Gelfand, A., Diggle, P., Fuentes, M., Guttorp, P., Eds.; CRC Press: Boca Raton, FL, 2010; pp 29−44.
(53) Zimmerman, D. L. Likelihood-Based Methods. In *Handbook of Spatial Statistics*; Gelfand, A. E., Diggle, P. J., Fuentes, M., Guttorp, P., Eds.; CRC Press: Boca Raton, FL, 2010; pp 45−56.
(54) Schielzeth, H. Simple Means to Improve the Interpretability of Regression Coefficients. *Methods Ecol. Evol.* **2010**, *1* (2), 103−113.
(55) Beale, C. M.; Lennon, J. J.; Yearsley, J. M.; Brewer, M. J.; Elston, D. A. Regression Analysis of Spatial Data. *Ecol. Lett.* **2010**, *13* (2), 246−264.
(56) Genton, M. G. Separable Approximations of Space-Time Covariance Matrices. *Environmetrics* **2007**, *18* (7), 681−695.
(57) Jat, P.; Serre, M. L. Bayesian Maximum Entropy Space/Time Estimation of Surface Water Chloride in Maryland Using River Distances. *Environ. Pollut.* **2016**, *219*, 1148−1155.
(58) NCDENR. *Surface Waters and Wetland Standards*; North Carolina Department of Environment and Natural Resources Division of Water Quality: Raleigh, North Carolina, USA, 2007; http://portal.ncdenr.org/c/document_library/get_file?uuid=f12e8078-b128-44cc-b55b-fc5e7d876f3c&groupId=38364.
(59) Neill, A. J.; Tetzlaff, D.; Strachan, N. J. C.; Hough, R. L.; Avery, L. M.; Watson, H.; Soulsby, C. Using Spatial-Stream-Network Models and Long-Term Data to Understand and Predict Dynamics of Faecal Contamination in a Mixed Land-Use Catchment. *Sci. Total Environ.* **2018**, *612*, 840−852.
(60) Peterson, E. E.; Ver Hoef, J. M.; Isaak, D. J.; Falke, J. a.; Fortin, M.-J.; Jordan, C. E.; McNyset, K.; Monestiez, P.; Ruesch, A. S.; Sengupta, A.; et al. Modelling Dendritic Ecological Networks in Space: An Integrated Network Perspective. *Ecol. Lett.* **2013**, *16* (5), 707−719.
(61) Peterson, E. E.; Urquhart, N. S. Predicting Water Quality Impaired Stream Segments Using Landscape-Scale Data and a Regional Geostatistical Model: A Case Study in Maryland. *Environ. Monit. Assess.* **2006**, *121* (1−3), 615−638.
(62) Peterson, E. E.; Merton, A. A.; Theobald, D. M.; Urquhart, N. S. Patterns of Spatial Autocorrelation in Stream Water Chemistry. *Environ. Monit. Assess.* **2006**, *121* (1−3), 571−596.
(63) Isaak, D. J.; Peterson, E. E.; Ver Hoef, J. M.; Wenger, S. J.; Falke, J. A.; Torgersen, C. E.; Sowder, C.; Steel, E. A.; Fortin, M.-J.; Jordan, C. E.; et al. Applications of Spatial Statistical Network Models to Stream Data. *Wiley Interdiscip. Rev.: Water* **2014**, *1* (3), 277−294.
(64) Som, N. a.; Monestiez, P.; Ver Hoef, J. M.; Zimmerman, D. L.; Peterson, E. E. Spatial Sampling on Streams: Principles for Inference on Aquatic Networks. *Environmetrics* **2014**, *25* (5), 306−323.
(65) Cho, K. H.; Cha, S. M.; Kang, J.-H.; Lee, S. W.; Park, Y.; Kim, J.-W.; Kim, J. H. Meteorological Effects on the Levels of Fecal Indicator Bacteria in an Urban Stream: A Modeling Approach. *Water Res.* **2010**, *44* (7), 2189−2202.
(66) Nash, M. S.; Heggem, D. T.; Ebert, D.; Wade, T. G.; Hall, R. K. Multi-Scale Landscape Factors Influencing Stream Water Quality in the State of Oregon. *Environ. Monit. Assess.* **2009**, *156* (1−4), 343−360.
(67) Whitman, R. L.; Przybyla-Kelly, K.; Shively, D. A.; Nevers, M. B.; Byappanahalli, M. N. Sunlight, Season, Snowmelt, Storm, and Source Affect E. Coli Populations in an Artificially Ponded Stream. *Sci. Total Environ.* **2008**, *390* (2−3), 448−455.
(68) Kang, J.-H.; Lee, S. W.; Cho, K. H.; Ki, S. J.; Cha, S. M.; Kim, J. H. Linking Land-Use Type and Stream Water Quality Using Spatial Data of Fecal Indicator Bacteria and Heavy Metals in the Yeongsan River Basin. *Water Res.* **2010**, *44* (14), 4143−4157.
(69) Mallin, M. a M.; Williams, K. E. K.; Esham, E. C.; Lowe, R. P. Effect of Human Development on Bacteriological Water Quality in Coastal Watersheds. *Ecol. Appl.* **2000**, *10* (4), 1047−1056.
(70) Korajkic, A.; McMinn, B. R.; Shanks, O. C.; Sivaganesan, M.; Fout, G. S.; Ashbolt, N. J. Biotic Interactions and Sunlight Affect Persistence of Fecal Indicator Bacteria and Microbial Source Tracking Genetic Markers in the Upper Mississippi River. *Appl. Environ. Microbiol.* **2014**, *80* (13), 3952−3961.
(71) Davies-Colley, R. J.; Bell, R. G.; Donnison, A. M. Sunlight Inactivation of Enterococci and Fecal Coliforms in Sewage Effluent Diluted in Seawater. *Appl. Environ. Microbiol.* **1994**, *60* (6), 2049−2058.
(72) Whitman, R. L.; Nevers, M. B.; Korinek, G. C.; Byappanahalli, M. N. Solar and Temporal Effects on Escherichia Coli Concentration at a Lake Michigan Swimming Beach Solar and Temporal Effects on Escherichia Coli Concentration at a Lake Michigan Swimming Beach †. *Appl. Environ. Microbiol.* **2004**, *70* (7), 4276.
(73) Thupaki, P.; Phanikumar, M. S.; Beletsky, D.; Schwab, D. J.; Nevers, M. B.; Whitman, R. L. Budget Analysis of Escherichia Coli at a Southern Lake Michigan Beach. *Environ. Sci. Technol.* **2010**, *44* (3), 1010−1016.
(74) Nguyen, T. D.; Thupaki, P.; Anderson, E. J.; Phanikumar, M. S. Summer Circulation and Exchange in the Saginaw Bay-Lake Huron System. *J. Geophys. Res. Ocean.* **2014**, *119* (4), 2713−2734.
(75) Annear, R. L.; Wells, S. A. A Comparison of Five Models for Estimating Clear-Sky Solar Radiation. *Water Resour. Res.* **2007**, *43* (10), W10415.

DOI: 10.1021/acs.est.8b01178
Environ. Sci. Technol. 2018, 52, 7775−7784

Geostatistical prediction of microbial water quality throughout a stream network using meteorology, land cover, and spatiotemporal autocorrelation: Supporting Information

David A. Holcomb, Kyle P. Messier, Marc L. Serre, Jakob G. Rowny, Jill R. Stewart

This supporting information contains 17 pages, 4 tables, and 3 figures.

Table of Contents

S.1 Profiling for Maximum Likelihood Estimation of Space/Time Model Parameters

The log-likelihood function for the Gaussian geostatistical model with n observations, mean function $(\boldsymbol{A\beta})$, and an error function with parameters $(\boldsymbol{\theta})$ yielding the covariance matrix $\left(\Sigma(\boldsymbol{\theta})\right)$, is given by

$$\ln L(\boldsymbol{\beta}, \boldsymbol{\theta}; \boldsymbol{Y}) = -\frac{n}{2}\ln(2\pi) - \frac{1}{2}\ln|\boldsymbol{\Sigma}(\boldsymbol{\theta})| - \frac{1}{2}(\boldsymbol{Y} - \boldsymbol{A\beta})^{\mathrm{T}}\boldsymbol{\Sigma^{-1}}(\boldsymbol{\theta})(\boldsymbol{Y} - \boldsymbol{A\beta}) \tag{S1}$$

where the response $(\boldsymbol{Y})$ is the natural logarithm transformed fecal coliform concentrations.[1] The values of $\boldsymbol{\beta}$ and $\boldsymbol{\theta}$ that maximize $\ln L(\boldsymbol{\beta}, \boldsymbol{\theta}; \boldsymbol{Y})$ are designated the maximum likelihood estimates (MLE), $\widehat{\boldsymbol{\beta}}$ and $\widehat{\boldsymbol{\theta}}$. Numerical approximation is used to obtain the MLE, as closed-form solutions to the likelihood function generally do not exist. To reduce the number of parameters that must be approximated, we recognize that the MLE of $\boldsymbol{\beta}$ for a given $\boldsymbol{\theta}$ is the generalized least squares (GLS) estimate given by

$$\widehat{\boldsymbol{\beta}} = (\boldsymbol{A}^T\boldsymbol{C^{-1}}(\boldsymbol{\theta})\boldsymbol{A})^{-1}\boldsymbol{A}^T\boldsymbol{C^{-1}}(\boldsymbol{\theta})\boldsymbol{Y} \tag{S2}$$

for the correlation matrix $\boldsymbol{C}(\boldsymbol{\theta})$, where $\boldsymbol{\Sigma}(\boldsymbol{\theta}) = \hat{\sigma}^2\boldsymbol{C}(\boldsymbol{\theta})$ and $\hat{\sigma}^2$ is the GLS variance estimate given by $\hat{\sigma}^2 = \left(\boldsymbol{Y} - \boldsymbol{A}\widehat{\boldsymbol{\beta}}\right)^{\mathrm{T}}\boldsymbol{C^{-1}}(\boldsymbol{\theta})(\boldsymbol{Y} - \boldsymbol{A}\widehat{\boldsymbol{\beta}})/n$. Numerical approximation is now required only to obtain MLE for $\boldsymbol{\theta}$, accomplished by maximizing the profile log-likelihood function

$$\ln L(\boldsymbol{\theta}; \boldsymbol{Y}) = -\frac{1}{2}\ln|\hat{\sigma}^2\boldsymbol{C}(\boldsymbol{\theta})| - \frac{1}{2}\left(\boldsymbol{Y} - \boldsymbol{A}\widehat{\boldsymbol{\beta}}\right)^{\mathrm{T}}(\widehat{\boldsymbol{\sigma}}^{\boldsymbol{2}}\boldsymbol{C}(\boldsymbol{\theta}))^{-1}(\boldsymbol{Y} - \boldsymbol{A}\widehat{\boldsymbol{\beta}}) \tag{S3}$$

using an iterative search algorithm. The algorithm is initialized with arbitrary starting values for $\boldsymbol{\theta}$ to calculate $\boldsymbol{C}(\boldsymbol{\theta})$, given below in (S4). From $\boldsymbol{C}(\boldsymbol{\theta})$ we obtain $\widehat{\boldsymbol{\beta}}$ and $\hat{\sigma}^2$, permitting the calculation of $\ln L(\boldsymbol{\theta}; \boldsymbol{Y})$ according to (S3). We approximate the MLE $(\widehat{\boldsymbol{\theta}})$ by repeating this process with different starting values for $\boldsymbol{\theta}$ and selecting the set of values that maximize $\ln L(\boldsymbol{\theta}; \boldsymbol{Y})$.

We used the *optim()* function in **R** to solve for the error function values that minimized $-\ln L(\boldsymbol{\theta}; \boldsymbol{Y})$, where $\boldsymbol{\theta} = [\alpha_s, \alpha_t, \tau]^T$, the spatial range, temporal range, and error partition parameters, respectively. The error partition parameter (τ) was used to apportion the GLS variance $(\hat{\sigma}^2)$ between the Euclidean partial sill (σ_e^2), which represents the correlated error proportion, and the nugget partial sill (σ_n^2), representing the uncorrelated error proportion. The partial sill estimates were calculated as $\hat{\sigma}_n^2 = \hat{\sigma}^2 \frac{\hat{\tau}}{1+\hat{\tau}}$ and $\hat{\sigma}_e^2 = \hat{\sigma}^2 \left(1 - \frac{\hat{\tau}}{1+\hat{\tau}}\right) = \hat{\sigma}^2 - \hat{\sigma}_n^2$. The correlation matrix $(\boldsymbol{C})$ is given by

$$\boldsymbol{C} = \frac{\exp(-3\mathbf{D}/\alpha_e)\exp(-3\mathbf{T}/\alpha_t) + \tau\mathbf{I}}{1+\tau} \tag{S4}$$

for spatial distance matrix $(\boldsymbol{D})$, temporal distance matrix $(\boldsymbol{T})$, the identity matrix $(\boldsymbol{I})$.

S.2 Universal Kriging Prediction Error Approximation

The universal kriging prediction variance (the square of the prediction error) is given by

$$\hat{\sigma}_k^2 = \hat{\sigma}^2 - \boldsymbol{\Sigma_{kh}\Sigma_{hh}^{-1}\Sigma_{kh}^T} + \left(\boldsymbol{a_k} - \boldsymbol{A^T\Sigma_{hh}^{-1}\Sigma_{kh}^T}\right)^T (\boldsymbol{A^T\Sigma_{hh}^{-1}A})(\boldsymbol{a_k} - \boldsymbol{A^T\Sigma_{hh}^{-1}\Sigma_{kh}^T}) \tag{S5}$$

for the GLS model variance estimate $(\hat{\sigma}^2)$, the vector of prediction location covariate values $(\boldsymbol{a_k})$, observation covariance matrix $(\boldsymbol{\Sigma}_{hh})$, and cross-covariance vector $(\boldsymbol{\Sigma}_{kh})$.[2] The term $\hat{\sigma}^2 - \boldsymbol{\Sigma_{kh}\Sigma_{hh}^{-1}\Sigma_{kh}^T}$ is the prediction variance for simple kriging, which is the best unbiased linear predictor when the mean at the prediction location (s_k) is known. In universal kriging, the mean at s_k is unknown and is obtained from the GLS estimate of the linear predictor as $\boldsymbol{a_k^T\hat{\beta}}$. The term $\left(\boldsymbol{a_k} - \boldsymbol{A^T\Sigma_{hh}^{-1}\Sigma_{kh}^T}\right)^T (\boldsymbol{A^T\Sigma_{hh}^{-1}A})(\boldsymbol{a_k} - \boldsymbol{A^T\Sigma_{hh}^{-1}\Sigma_{kh}^T})$ in the universal kriging variance penalizes the simple kriging variance for the uncertainty introduced by estimating $\boldsymbol{\hat{\beta}}$. As such, the simple kriging variance $\hat{\sigma}_k^2 = \hat{\sigma}^2 - \boldsymbol{\Sigma_{kh}\Sigma_{hh}^{-1}\Sigma_{kh}^T}$ is the lower bound of, and may serve as a convenient

approximation for, the universal kriging variance. The square root of the kriging variance yields the prediction standard error.

S.3 Calculation of Additive Function Values for Flow-Weighting

An additive step function was used to represent downstream flow connection in the stream network, in which each stream segment is assigned an additive function value (AFV). We derived the AFVs from the non-overlapping catchment area of each stream segment, which serves as a proxy for the flow contributed by the segment. Under this construction, a flow weight is assigned to each downstream segment equal to the sum of flow-contributing upstream segment AFVs. **STARS** tools were used to delineate stream segment catchments from the DEM and calculate the catchment areas (A_i). Where two stream segments i and j join, each is assigned a segment proportional influence (PI) weight $\left(\omega_i = \frac{A_i}{A_i + A_j}\right)$, such that the PIs at each junction sum to 1. Each segment is assigned an AFV corresponding to the product of the downstream segment PIs, a value between 0 and 1. Each sample location and estimation point is assigned the AFV of the underlying stream segment.

S.4 Exploratory Analysis of Input Variables

Table S1 presents summary statistics for the input variables used to fit geostatistical models of fecal coliform concentration. Input variables are divided into the following three categories: the response, measured directly in water samples; land cover predictors, derived from remote sensing and digital elevation model (DEM) delineated upstream watersheds; and meteorological predictors, derived from hourly measurements at a single weather station representing the entire study area. The geometric mean of all the fecal coliform concentrations was 219.1 cfu/100 mL, which slightly exceeds the North Carolina state water quality standard for

Type C surface waters, set at a fecal coliform geometric mean of 200 cfu/100 mL measured in at least 5 water samples.

Table S1. Summary statistics for response and predictor variables.

Variable (units)	**Mean**	**Standard Deviation**	**Median**	**Minimum**	**Maximum**
Response					
Fecal coliform concentration (cfu/100 mL)	1713.8	6216.2	166.9	1.2	97200
Land cover predictors					
Impervious surface (% upstream watershed area)	12.8	10.2	9.7	0.4	40.6
Water (% upstream watershed area)	0.39	0.32	0.25	0	0.95
Forest (% upstream watershed area)	41.1	21.5	42.8	0	74.0
Agriculture (% upstream watershed area)	5.4	5.2	2.5	0	19.3
Meteorological predictors					
Solar radiation (W/m^2)	212.1	215.5	140.5	9.0	859.5
Surface temperature (°C)	18.23	10.3	19.0	-7.8	45.3
0 – 2 day prior precipitation (mm)	12.3	25.0	0.25	0	98.4
2 – 7 day prior precipitation (mm)	16.6	24.8	7.0	0	115.3

S.5 Visual Interpretation of the Error Function

The error function in a geostatistical model describes the decay of covariance between realizations of the response variable associated with increasing distance between the locations of the realizations in space (and time, in space/time models). Plotting the modeled covariance against this distance, referred to as the spatial (or temporal) lag, allows for visualization of the relationship between covariance and distance modeled in the error function. Figure S1 presents error function graphs for two of the four models we considered, the Euclidean space-only model and the Euclidean space/time model, for which the spatial and temporal components are presented separately. The two other models, stream distance and flow-weighted stream distance, both combine a Euclidean distance component and a stream distance component, which prevents depiction of their respective error functions. Because the Euclidean distance component dominated in both the stream distance and flow-weighted stream distance models, in practice the error function for both would closely resemble that of the Euclidean space-only model. The ordinary least squares (OLS) model assumes all uncorrelated error and as such has no distance-based relationship to be displayed.

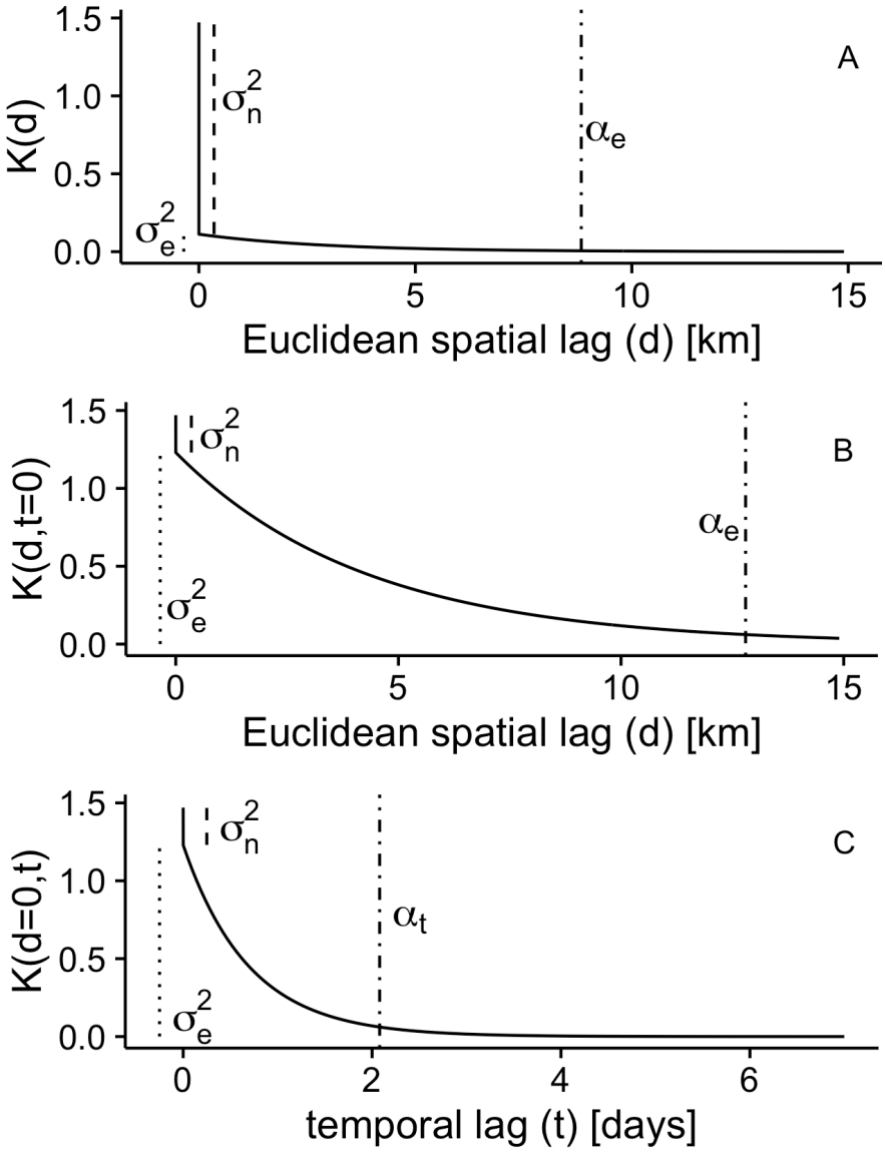

Figure S1. Error function graphs of covariance distance-decay relationship for the space-only model (panel A), space/time model spatial component (panel B), and space/time model temporal component (panel C). The vertical axis is the modeled covariance in ln(FC) response, in units of ln(fc)^2/100 mL. The nugget (uncorrelated error) partial sill σ_n^2 is represented in all three graphs as a dashed vertical line, the length of which corresponds to the maximum likelihood estimate of σ_n^2. Similarly, the Euclidean distance partial sill σ_e^2 is represented as a vertical dotted line. The spatial range α_e, the Euclidean spatial lag value at which the spatial covariance is reduced to 5% of its initial value, is presented in panels A and B as dot-dashed lines intersecting the horizontal axis at the value of the maximum likelihood estimate of α_e. The temporal range α_t is likewise displayed in panel C.

S.6 Mean Function Parameter Estimates

The structure of the mean function was the same for each of the five models we fit, but the different error function for each model slightly affected the mean function parameter estimates. The mean functions for all five models had approximately the same explanatory capability, however, each accounting for 59% of the total variance in the data. Standardized (mean-centered, standard deviation-scaled) values of the input variables were used to enhance interpretability of the parameter estimates reported in Figure 2, but such linear transformations do not affect the overall fit or predictive performance of the model. Here we fit the models to the untransformed values of the input variables, which produces parameter estimates corresponding the expected change in ln(FC) concentration for a one-unit increase in the predictor value, when all other variables are held constant. (As with the standardized inputs, this interpretation does not hold for the precipitation terms, which are related through the interaction term; see next section in Supporting Information for explanation.) Table S2 presents the mean function parameter estimates for the ordinary least squares (OLS), Euclidean distance-only spatial ("space-only"), stream distance spatial ("stream distance"), flow-weighted stream distance spatial ("flow-weighted"), and Euclidean separable spatiotemporal ("space/time") models. Note the nearly equivalent parameter estimates for the space, stream, and flow-weighted models, which have very similar error functions due to the negligible partial sills for non-Euclidean components in the stream distance and flow-weighted models.

Table S2. Mean function parameter estimates for each of the five models considered.

Predictor (units)	**Parameter**	**OLS model estimate** $\left(\mathbf{SE}^{*}, \boldsymbol{P}(>\lvert\mathbf{t}\rvert)\right)$	**Space-only model estimate** $\left(\mathbf{SE}, \boldsymbol{P}(>\lvert\mathbf{t}\rvert)\right)$	**Stream distance model estimate** $\left(\mathbf{SE}, \boldsymbol{P}(>\lvert\mathbf{t}\rvert)\right)$	**Flow-weighted model estimate** $\left(\mathbf{SE}, \boldsymbol{P}(>\lvert\mathbf{t}\rvert)\right)$	**Space/time model estimate** $\left(\mathbf{SE}, \boldsymbol{P}(>\lvert\mathbf{t}\rvert)\right)$
Intercept (ln(cfu)/100 mL)	β_0	4.71 (0.15, <0.001)	4.68 (0.24, <0.001)	4.68 (0.24, <0.001)	4.68 (0.24, <0.001)	4.76 (0.19, <0.001)
Forested (%)	β_1	-0.033 (0.0050, <0.001)	-0.033 (0.0087, <0.001)	-0.033 (0.0087, <0.001)	-0.032 (0.0088, <0.001)	-0.030 (0.0049, <0.001)
Agricultural (%)	β_2	0.074 (0.021, <0.001)	0.066 (0.037, 0.07)	0.066 (0.037, 0.07)	0.062 (0.037, 0.1)	0.066 (0.021, <0.001)
Surface temperature (°C)	β_3	0.043 (0.0047, <0.001)	0.046 (0.0046, <0.001)	0.046 (0.0046, <0.001)	0.046 (0.0046, <0.001)	0.035 (0.0070, <0.001)
0 – 2 day prior precipitation (mm)	β_4	0.072 (0.0046, <0.001)	0.072 (0.0044, <0.001)	0.072 (0.0044, <0.001)	0.072 (0.0044, <0.001)	0.067 (0.0068, <0.001)
2 – 7 day prior precipitation (mm)	β_5	0.017 (0.0024, <0.001)	0.017 (0.0023, <0.001)	0.017 (0.0023, <0.001)	0.017 (0.0023, <0.001)	0.017 (0.0035, <0.001)
Precipitation interaction (mm^2)	β_6	-0.00059 (0.000090, <0.001)	-0.00060 (0.000076, <0.001)	-0.00060 (0.000076, <0.001)	-0.00060 (0.000076, <0.001)	-0.00052 (0.00013, <0.001)

*standard error of the parameter estimate

The reduced set of predictor variables used to compare models was selected from the candidate predictors described in Table S1. We fit the flow-weighted model using the full set of predictors excepting water cover, which accounted for less than 1% of the area in all upstream watersheds. Table S3 shows the mean function parameter estimates for the full set of predictors under the flow-weighted model, which yielded an AIC of 2194, an R^2 value of 0.60, and an RSME of 1.19 log(cfu)/100 mL. The reduced predictor set was selected by backwards elimination using the criterion of minimizing AIC.

Table S3. Flow-weighted model mean function parameter estimates for the full set of predictors.

Predictor	**Units**	**Parameter Estimate**	**Standard Error**	$\boldsymbol{P(>\lvert t\rvert)}$
Intercept	$\frac{\ln(\text{cfu})}{100\text{ mL}}$	4.32	0.65	< 0.001
Impervious surface	%	0.013	0.019	0.51
Forested	%	-0.024	0.013	0.07
Agricultural	%	0.048	0.038	0.20
Solar radiation	W/m^2	-0.0002	0.0003	0.43
Surface temperature	°C	0.048	0.0055	< 0.001
0 – 2 day prior precipitation	mm	0.071	0.0044	< 0.001
2 – 7 day prior precipitation	mm	0.017	0.0023	< 0.001
Precipitation interaction	mm^2	-0.0006	0.00008	< 0.001

S.7 Derivation of Precipitation Interaction Effects

Consider the general geostatistical model for a single observation y_i with precipitation terms separated out:

$$y_i = \boldsymbol{a_{i,1-3}\beta_{1-3}} + \beta_4 a_{i,4} + \beta_5 a_{i,5} + \beta_6 a_{i,4} a_{i,5} + z_i \quad (6)$$

where β_4 and $a_{i,4}$ correspond to 0 – 2 day prior precipitation ("new rain") parameter estimate and observed value at point i, β_5 and $a_{i,5}$ to 2 – 7 day prior precipitation ("old rain") parameter estimate and observed value, and β_6 is the parameter for their interaction ("rain interaction"). To calculate the total effect of new rain, we rearrange the model as

$$y_i = \boldsymbol{a_{i,1-3}\beta_{1-3}} + \beta_4 a_{i,4}\left(1 + \frac{\beta_6}{\beta_4} a_{i,5}\right) + \beta_5 a_{i,5} + z_i \quad (7)$$

For positive new rain main effect β_4 and negative rain interaction effect β_6 (as estimated in all four of our models), the result is a diminished total effect of new rain for increasing values of old rain $a_{i,5}$.

S.8 Prediction at Individual Sampling Sites

We assessed the performance of all five models using leave-one-out cross validation, in which each observation is removed in turn and predicted from predictor values and the remaining observed concentrations. For each space/time point in the data set, LOOCV produces a pair of observed and predicted FC concentrations, the difference between which constitutes the prediction error. The mean of the squared prediction errors for a given dataset provides a useful metric by which to evaluate the accuracy of a model's predictions; the positive root of this value yields the root mean squared error on the same scale as the original data. A related metric, the corrected prediction R^2, uses the prediction error to account for the proportion of the total variance in the data that is explained by the model, corrected for the variance that is explained by substituting the grand mean of the data for each prediction.

With the goal of predicting FC throughout the spatiotemporal domain of our study area, we used all 676 FC observations to fit each of the five models considered. We evaluated predictive performance for each model primarily on the basis of RMSE for the full dataset, which indicates the average predictive performance across the study domain. However, the observations were collected from 19 distinct sampling sites between 24 and 79 times per site, and each LOOCV prediction was made for one site at a particular sampling time. Because the space/time model performed best in terms of both RSME and corrected prediction R^2 for the full dataset, we further evaluated its performance for each sampling site considered individually. Figure S2 shows the correspondence between observed FC concentrations and those predicted by the space/time model for each sampling site, as well as for all sites considered collectively. Points falling above the dashed line in the center of each plot were overpredicted, points below the line were underpredicted, and increasing distance from the line indicates greater prediction

error. Prediction accuracy varied by site, with RSME ranging from 0.61 – 1.48 ln(cfu)/100 mL (Table S4), compared with an RSME of 1.02 ln(cfu)/100 mL for all sites together. Site-specific model performance was apparently unaffected by the number of observations at any given site.

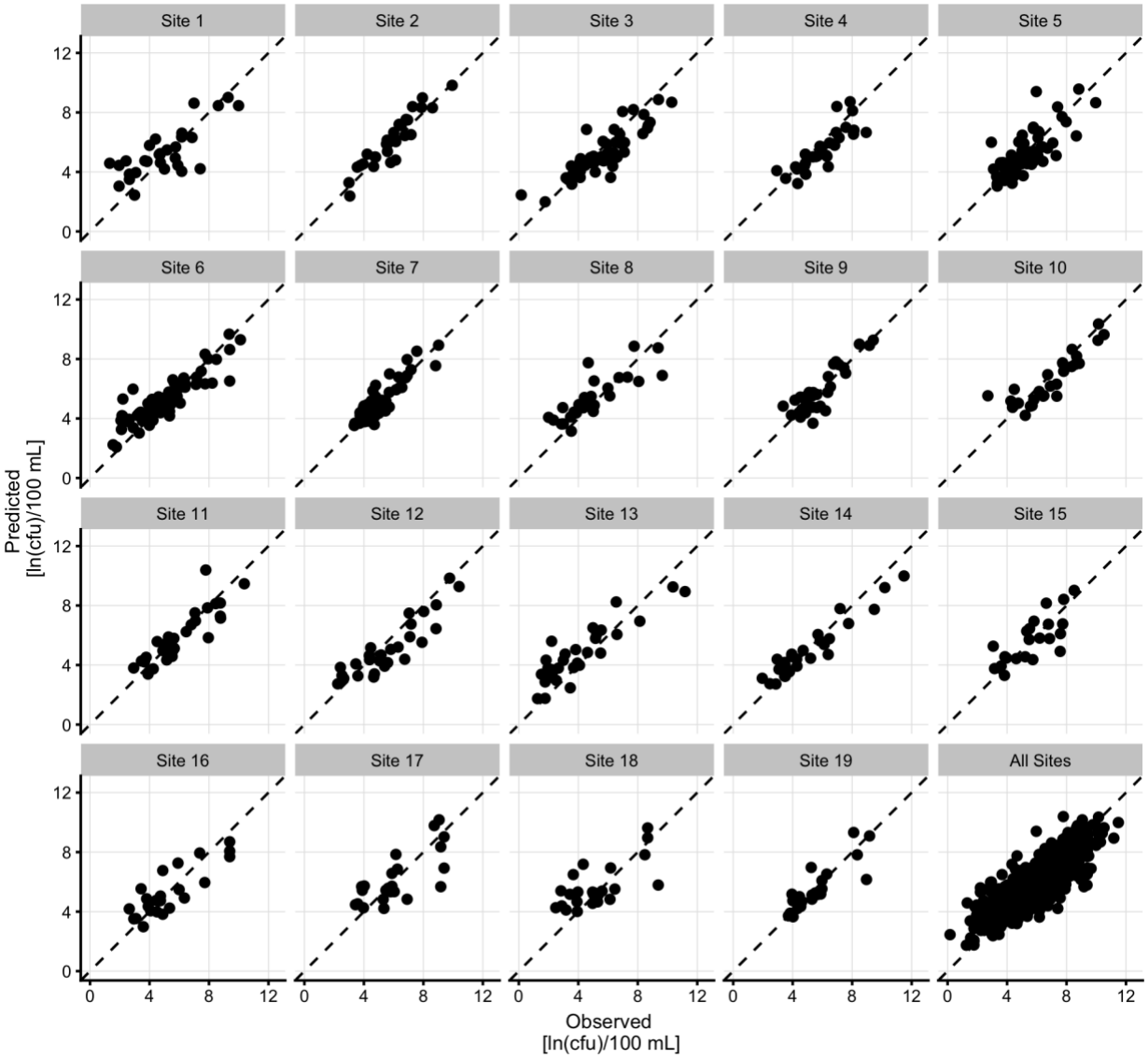

Figure S2. Comparison of predicted FC with observed concentrations at each sample site and for all sites in aggregate. Dashed line represents a 1:1 correspondence between observed and predicted FC concentration.

Table S4. Space/time model predictive performance under LOOCV at each sampling site.

Site ID	Latitude (°N)	Longitude (°E)	n	RMSE [ln(cfu)/100 mL]	R^2
1	35.923399	-79.115062	30	1.41	0.58
2	35.898559	-79.034915	30	0.64	0.85
3	35.898700	-79.026300	55	1.05	0.69
4	35.917767	-79.011277	30	0.96	0.63
5	35.861150	-79.010000	78	0.94	0.54
6	35.884740	-78.965630	79	0.97	0.76
7	35.872430	-78.913220	55	0.61	0.78
8	35.915389	-78.893528	27	1.20	0.64
9	35.922639	-78.952417	30	0.75	0.77
10	35.979550	-78.914850	26	1.00	0.84
11	35.983020	-78.957210	31	0.90	0.79
12	36.004367	-78.971167	29	1.12	0.74
13	35.979600	-79.001622	30	1.35	0.77
14	35.992217	-79.045687	28	0.81	0.88
15	35.943026	-79.057701	22	1.09	0.55
16	35.916700	-78.970400	24	1.08	0.71
17	35.918700	-78.954800	24	1.33	0.60
18	35.887020	-78.899430	24	1.48	0.42
19	35.855500	-78.939700	24	0.84	0.72

Considering predictions at individual sites across time further highlights the highly variable temporal trends in FC concentration. Figure S3 shows time series of daily kriging prediction means and 95% confidence intervals at three sampling sites, overlaid with observed FC concentrations and their corresponding LOOCV predictions. The displayed sites represent relatively strong (Figure S3(a) – Site 7), weak (Figure S3(b) – Site 13), and moderate (Figure S3(c) – Site 16) prediction performance by RMSE. The daily kriging prediction means do not necessarily match the LOOCV predictions for the same day because they incorporate the site-specific observations excluded under LOOCV. Though the magnitudes may differ, the direction of concentration trends were similar for all three sites, reflecting the powerful influence of precipitation (which is the same for all sites at a given time) on predictions. The correspondence

in FC trend between sites held in the absence of observational data. On multiple occasions at each site, the model predicted FC concentrations exceeding the NC standard (5.3 ln(cfu)/100 mL) without FC observations to draw on. While the prediction uncertainty in such instances generally increased to the point that impairment could not be diagnosed with high probability (illustrated by wider confidence bands in Figure S3), the ability to predict elevated FC without requiring additional samples demonstrates the potential for the model to inform watershed management.

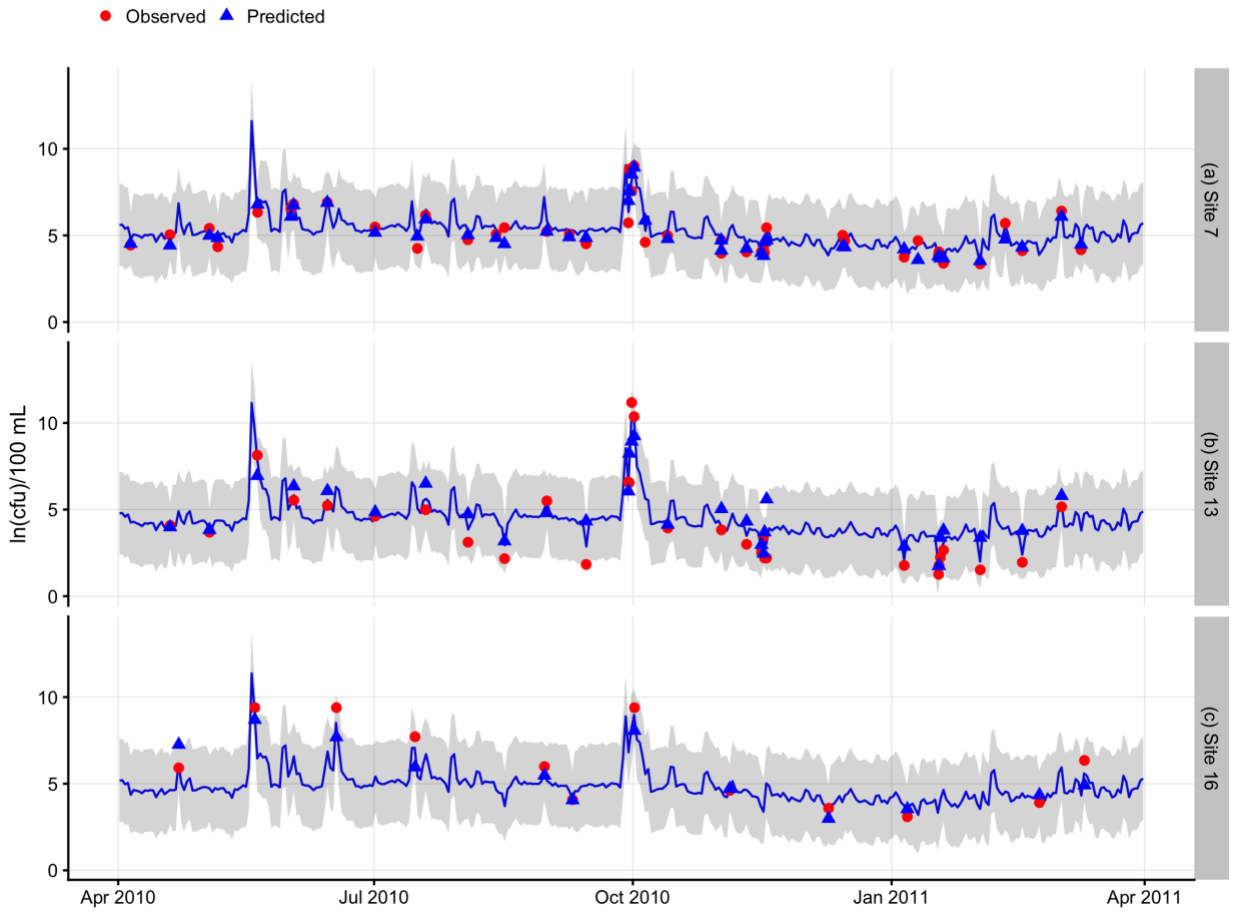

Figure S3. Time series of FC observations (red circles), corresponding space/time model predictions (blue triangles), and daily FC prediction mean (blue line) and 95% confidence interval (gray shading) for selected sampling sites. The selected sites demonstrate high performance (a), low performance (b), and moderate performance (c) in terms of RMSE, relative to the other sites.

S.9 Animated Maps of Daily Watershed Predictions

We compiled three time-lapsed animations mapping kriging prediction means, standard errors, and impairment status, respectively, for 11:00 a.m. on each of the 365 study days falling between April 1, 2010 and March 31, 2011. They may be viewed free of charge online at the following website: http://www.unc.edu/depts/case/BMElab/studies/DAH_FC_Jordan/, and individual animations may be accessed directly at the following addresses:

- *Kriging prediction means*, http://www.unc.edu/depts/case/BMElab/studies/DAH_FC_Jordan/means.gif
- *Kriging prediction standard errors*, http://www.unc.edu/depts/case/BMElab/studies/DAH_FC_Jordan/errors.gif
- *Predicted watershed impairment status*, http://www.unc.edu/depts/case/BMElab/studies/DAH_FC_Jordan/impairment.gif

References

(1) Zimmerman, D. L. Likelihood-Based Methods. In *Handbook of Spatial Statistics*; Gelfand, A. E., Diggle, P. J., Fuentes, M., Guttorp, P., Eds.; CRC Press: Boca Raton, FL, 2010; pp 45–56.

(2) Zimmerman, D. L.; Stein, M. Classical Geostatistical Methods. In *Handbook of Spatial Statistics*; Gelfand, A., Diggle, P., Fuentes, M., Guttorp, P., Eds.; CRC Press: Boca Raton, FL, 2010; pp 29–44.